Understanding protein complex formation: the role of charge distribution in the encounter complex

Di Savino, A.

Chapter 3

Efficient encounter complex formation and electron transfer to cytochrome *c* peroxidase with an additional, distant electrostatic binding site.

Based on the research article:

Di Savino, A., Foerster, J., La Haye, T., Blok, A., Timmer, M., Ullmann, M., and Ubbink, M. (2020) Efficient encounter complex formation and electron transfer to cytochrome *c* peroxidase with an additional, distant electrostatic binding site. Angew. Chemie Int. Ed. 132, 23239–23243.

Chapter 3

Abstract

Electrostatic interactions can strongly increase the efficiency of protein complex formation. The charge distribution in redox proteins is often optimized to steer a redox partner to the electron transfer active binding site. To test whether the optimized distribution is more important than the strength of the electrostatic interactions, an additional negative patch was introduced on the surface of cytochrome *c* peroxidase, away from the stereospecific binding site, and its effect on the encounter complex as well as the rate of complex formation was determined. Monte Carlo simulations and paramagnetic relaxation enhancement NMR experiments indicate that the partner, cytochrome *c*, interacts with the new patch. Unexpectedly, the rate of the active complex formation was not reduced, but rather slightly increased. The findings support the idea that for efficient protein complex formation the strength of the electrostatic interaction is more critical than an optimized charge distribution.

Introduction

Electrostatic interactions are fundamental in protein-protein interactions and formation of protein complexes. Charge-charge interactions guide the recognition and binding between proteins and between a protein and a ligand.[1-5] Before forming the stereospecific, active complex, proteins associate into an intermediate state, the encounter complex, consisting of an ensemble of transient conformations, in which the proteins sample the surface of the partner.[6] The encounter complex is thought to reduce the dimensionality of the search for the binding site.[7] During this process electrostatic interactions contribute to pre-organization of the protein orientations in the encounter complex, reducing the surface area to be sampled and promoting the formation of the stereospecific complex. The encounter complex formation is initially mostly driven by long-range electrostatic interactions. Upon closer approach of the two proteins, hydrophobic interactions also come into play, ultimately leading to the formation of the stereospecific complex.[8-15] The association rate constant, the measure for productive complex formation, can be four orders of magnitude lower than the diffusional collision rate constant in cases in which complex formation is not optimized, indicating that most encounters are non-productive and partners dissociate before reaching the stereospecific complex. Such encounters are called futile.[16, 17] On the other hand, association rate constants approach the collision rate constant for some complexes, which is thought to be caused by strong electrostatic pre-organization of the encounter complexes, with the charge interactions guiding the partners to the correct orientation for binding.[1] For such complexes, charge distribution over the surfaces of the proteins is expected to be optimized by evolution. The complex formed by cytochrome P450cam and putidaredoxin was previously studied to understand the function of the different encounter complexes formed by the two proteins. The data suggest that the encounter complexes located in a region with an electrostatically favorable pathway to the stereospecific binding site represent productive encounter states. On the contrary, encounter complexes located far from the binding site and in absence of a favorable charged path that extends to the binding site consist of futile interactions.[18] The encounter complex is therefore a key stage in the formation of a protein complex and mutations that affect the encounter complex have consequences for the stereospecific protein complex. Previous studies by Harel *et al.*[16] on the interactions between TEM1-β-lactamase (TEM1) and its inhibitor, β-lactamase-inhibitor protein (BLIP), showed that it is difficult to define a correlation between the energy of the interaction, the surface area searched by the encounter complex and the association rate between two proteins. Recently, it was shown that futile encounter complexes could have a role in regulation of enzyme activity forming competitive encounter complexes.[19, 20] Interestingly, charge mutations on the protein surface far from the active site can either enhance complex formation by creating new productive encounter complexes, or decrease it by breaking diffusional pathways over the surface that would lead to the formation of the stereospecific complex.[21] We wondered how critical such a charge distribution is for fast complex formation in an optimized complex, as compared to the total strength of the electrostatic interactions. Good complexes to study this question are those formed by electron transfer (ET) proteins, as these are highly

transient, i.e. have a high association and dissociation rate constants, and the fraction of the encounter complex is high. The reason for these features is related to the biological function. Transfer of electrons in redox chains, such as found in photosynthesis and respiration, can be rate-limiting for the entire process and, thus, complex formation must be efficient. One of the best characterized ET complexes is the one formed by cytochrome *c* peroxidase (CcP) and cytochrome *c* (Cc) from baker's yeast (*Saccharomyces cerevisiae*). The formation of the encounter complex is driven by electrostatic interactions between positive charges on Cc and negative charges on CcP.[22-26] The encounter state and the stereospecific complex represent 30% and 70% of the complex, respectively.[27, 28] Due to the electrostatic pre-organization, the area sampled by Cc was estimated to be merely 15% of the CcP surface.[28] The fraction of encounter complex was found to be affected by mutations in the binding site, with the fraction of the encounter complex ranging from 10% to 90% for different mutations.[29] CcP catalyzes the reduction of H_2O_2 to water using electrons donated by reduced Cc. The reaction proceeds through a complicated cycle, during which two molecules of Cc interact with CcP sequentially, each contributing one electron (Text S3.2). In line with other ET complexes, the ET rate is high (>50,000 s^{-1})[30], the lifetime of the complex is short (0.1 - 1 ms)[31], the association rate constant very high (10^8 – 10^9 $M^{-1}s^{-1}$ at 200 mM ionic strength)[32] and the affinity in the micromolar range (K_D = 5 μM).[31] In a previous study by Erman and co-workers[33-35] several charge-reversal mutants of CcP were created to determine the impact of the charges on the surface of the protein on the association with Cc. The majority of these mutations, mainly the ones located in or around the binding site of Cc, significantly decreased the affinity between the two proteins. Interestingly, three of these mutations (D37K, E28K, and E209K) are slightly more distant from the binding site and two of them on the opposite side of the protein (D165K and D241K). Although it is possible that the mutation D241K could affect the stability of the protein, this study shows that the charged residues on the surface, also located far from the binding site, have a role in the association process of Cc and CcP.

To establish how important the optimization of the charge distribution on CcP is for achieving these ET specifications, we decided to change the charge distribution on the CcP surface by adding a new negative patch in addition to the existing one surrounding the binding site for Cc. The new patch interferes with the distribution of negative charge in native CcP that appears to be optimized for Cc honing into the stereospecific binding site. Thus, we expected that productive complex formation would be affected negatively, leading to more futile encounters. The interaction with this mutant CcP (CcP_B) was studied using Monte Carlo electrostatic calculations, paramagnetic relaxation enhancement (PRE) NMR spectroscopy and stopped-flow kinetic measurements to determine the association rate constant as a function of ionic strength. Both modelling and PRE-NMR demonstrate that the new negative patch is visited by Cc in the encounter state. Yet, to our surprise, the association rate is not reduced relative to the interaction with wild type CcP (CcP_A), and even appears to be enhanced slightly at moderate ionic strength. These observations indicate that the precise charge distribution around the binding site is less

critical for complex formation than expected and the increased strength of the electrostatic interactions may compensate for a less optimal encounter complex.

Results and Discussion

Monte Carlo simulations show Cc to interact with the added patch on CcP

To test how important the charge distribution of CcP is for binding and reduction by Cc, an additional negative patch was created on one side of the regular binding site for Cc, by changing four positive sidechains to negative ones (mutations K21E, K29E, K90E, and K97E), thus introducing a net charge change of -8 (Figure 3.1a, 3.1b). This construct, CcP_B, was characterized by Monte Carlo simulations, NMR spectroscopy and stopped-flow spectroscopy. Rigid-body Monte Carlo simulations, based only on electrostatic and steric interactions, were used to simulate the encounter complexes of Cc with wild type CcP (CcP_A) or CcP_B. Figure 3.1c shows CcP in ribbon representation and the ensemble of Cc centers-of-mass based on electrostatic interaction energies. The densest regions represent the most favorable Cc orientations. The interactions of Cc with CcP_A (cyan spheres) are predominantly found at the location of the stereospecific binding site, in accord with earlier calculations[23, 26, 28, 37] According to the simulations, the mutations introduced on the CcP_B surface considerably affect the encounter complex, with Cc sampling the area with the added negative charges of CcP_B (magenta spheres) more frequently than the crystallographic binding site. Note that these calculations only consider electrostatic interactions. In the stereospecific complex additional favorable interactions are present, so the total interaction is not expected to shift as dramatically as follows from these calculations. Still, it is clear that these extra negative charges should have a significant effect on the distribution of Cc in the encounter state.

Affinity and binding of Cc is similar for CcP_A and CcP_B

NMR titration experiments of Cc and CcP_A and CcP_B (S. I. Text S3.1 and Figure S3.1) show that the introduction of the additional charges has surprisingly little effect on the affinity and binding effects in the HSQC spectrum. It is noted that CSP are predominantly caused by the stereospecific complex and not by the encounter complex. In the latter, solvation is likely to be similar to that for free Cc and binding occurs in many orientations. Both factors contribute to minimal perturbations of the chemical environment of the amide groups observed in the HSQC experiment. Desolvation and a well-defined orientation in the stereospecific complex are expected to cause most of the CSP.[38-40] So it appears that the additional charges do not cause a major shift in the equilibrium between encounter state and stereospecific complex, reported to be 30%:70%,[27, 28] because that would have changed the overall size of the CSP. The extremely dynamic nature of the encounter complex and the fact that it is usually present in a small fraction of the protein-complex lifetime, makes it invisible to the conventional biophysical techniques used to study protein-protein

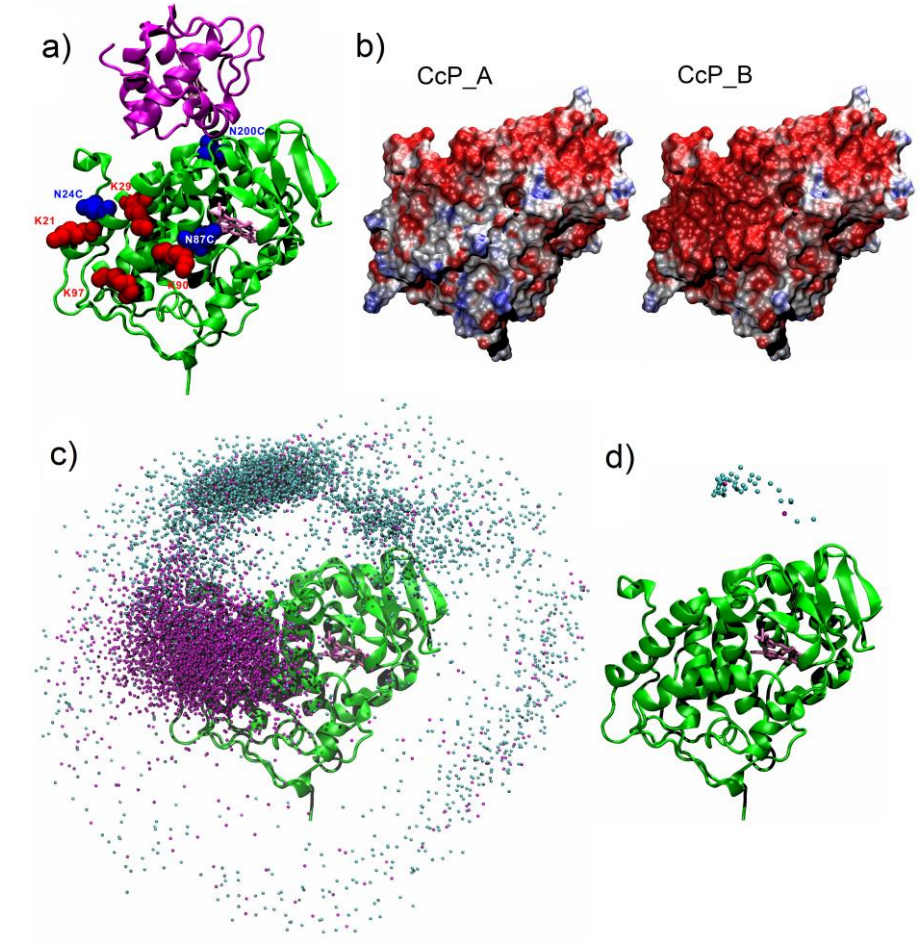

Figure 3.1. A new negative patch on CcP. a) Crystal structure of the stereospecific complex formed by Cc (magenta ribbons) and CcP (green ribbons) is shown (PDB 2PCC[22]). The heme groups are shown in pink sticks, the residues that were mutated to introduce additional negative charges in CcP_B are in red spacefilling representation and the residues mutated to cysteines for PRE experiments in blue spacefill. Electrostatic potential on the surface of CcP_A and CcP_B ranging from -5 (red) to 5 kcal/e^o (blue) at an ionic strength of 120 mM. c) The structure of CcP (green ribbon) is surrounded by the centers of the mass of Cc in the ensemble of encounters of the complexes Cc:CcP_A (cyan) and Cc:CcP_B (magenta) as obtained from rigid body Monte Carlo simulations. d) The structure of CcP (green ribbon) is surrounded by the centers of the mass of Cc in the ensemble of encounters of the complexes Cc:CcP_A (cyan) and Cc:CcP_B (magenta) in which the edge-to-edge distance between Cc heme and the indole of the CcP compound I radical forming Trp (Trp-191) is less than 1.6 nm, as obtained from rigid body Monte Carlo simulations. CcP is in the same orientation in all panels. The pictures were produced with VMD.[36]

structures.

PRE experiments demonstrate that Cc interacts with the new negative patch

To establish whether Cc visits the new negative patch in the encounter state, we employed paramagnetic relaxation enhancement (PRE) NMR spectroscopy. PRE are very sensitive to minor states in which a nucleus is closer to the paramagnetic center than in the major state, because of the large relaxation effect of unpaired electrons and the steep distance dependence of the effect (r^{-6}).[41, 42] To probe for such Cc interactions, two amino acids surrounding the new negative patch on CcP_B were individually mutated to cysteines (N87C and N24C, see Figure 3.1). These positions surround the new negative patch but are far from the regular Cc binding site. The mutations were also made in CcP_A. A third cysteine was introduced near the binding site of Cc (N200C) as a control. PRE data for this site have been reported before for the complex of CcP with WT Cc as well as several mutants.[29, 43] The cysteine residues were used for the attachment of the small, stable spin label MTSL that causes PRE in a sphere of up to 2.5 nm. The spin labelled CcP_B was mixed with ^{15}N labelled Cc to record intermolecular PRE, from the CcP spin label on the Cc nuclei. The spin labels on the mutants N87C, N24C, and N200C of CcP_B induced large PRE in Cc (Figure 3.2). Analogous experiments on CcP_A mutant spin labelled at N87C and N24C showed much smaller PRE (Figure 3.2),

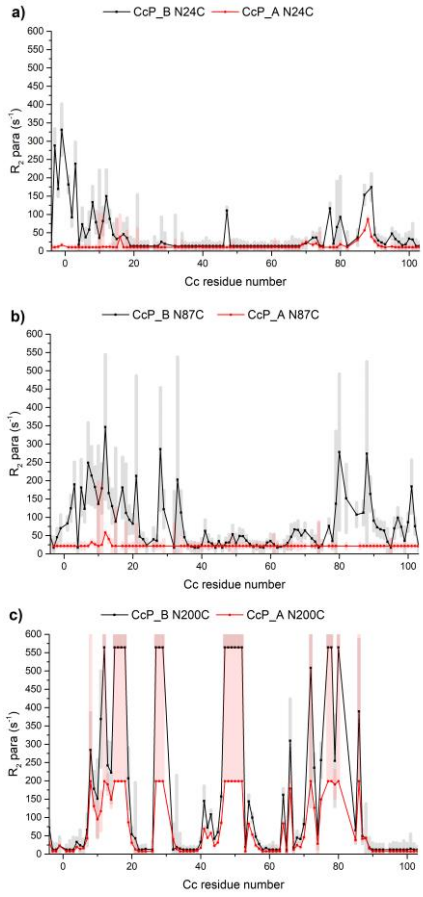

Figure 3.2. Probing new interactions with PRE NMR. The PRE on Cc in presence of CcP_A (in red) or CcP_B (in black), tagged with MTSL on N24C (a) and N87C (b), both located around the negative patch introduced in CcP_B, and N200C (c) close to the stereospecific binding site. The errors bars are indicated as shaded regions in red for Cc:CcP_A and in grey for Cc:CcP_B and represent the propagated 2 SD errors of the raw data. The upper and lower limit cut-offs for PRE differ between samples, depending on the fraction of CcP that was paramagnetic, as based on EPR measurements (see the Materials and Methods in the Supplementary Information section for details).

whereas the effects for N200C were similar to those for CcP_B and those reported before.[27] Thus, the large differences in PRE between CcP_A and CcP_B provide strong evidence that the new negative patch has become part of the encounter complex and is visited by Cc.

Binding at the new negative patch yields productive encounters

The aim of this project was to determine whether the charges involved in formation of the encounter complex need to surround the binding site for the stereospecific complex to achieve optimal electron transfer. The NMR results show that the encounter complex has changed in CcP_B, extending the encounter complex away from the stereospecific binding site. To monitor whether the formation of productive, i.e. electron transfer active, complexes is affected by the charges added to the surface of CcP_B, the association rate constant was determined by stopped-flow spectrometry, following early work of Miller *et al.*[32] In these experiments, CcP is first reacted with hydrogen peroxide to form the oxyferryl/Trp-radical species (compound I)[44-46] and then mixed rapidly with reduced Cc. The ensuing electron transfer from Cc(II) to compound I, forming Cc(III) and compound II,[47, 48] is followed in time as a change in Cc absorption at 416 nm (see Text S3.2). It can be shown that the observed second order rate constant is a lower limit of the association rate constant for productive complex formation, see equation 3 in the Experimental Procedures

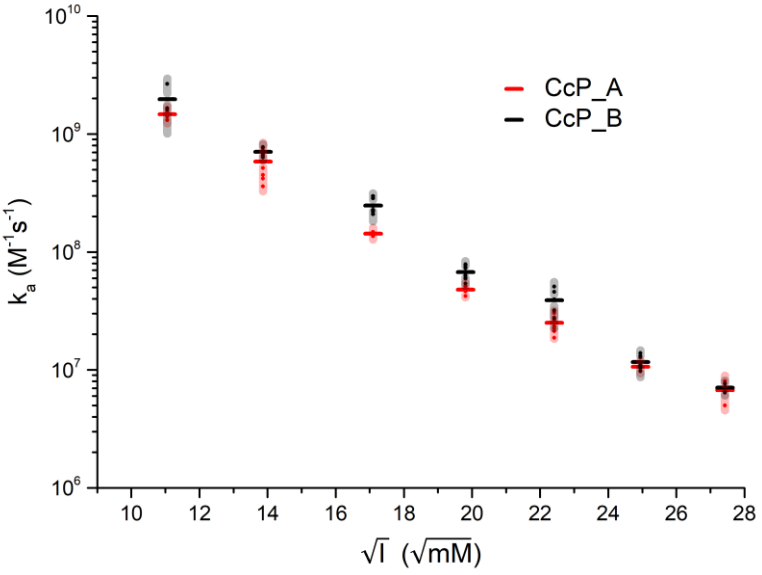

Figure 3.3. Association rate constants of Cc and CcP. The association rate constants (k_a) of the complexes Cc:CcP_A (red symbols) and Cc:CcP_B (black symbols) plotted as a function of the root of the ionic strength. The colored dots represent the k_a values obtained from fitting averages of 14 single measurements, while the bars represent the average of the dots. The errors in the rate constants are shown as shades and represent the standard deviation between the dots (see the Matherials and Methods section in the Supplementary Information for details).

in the Supplementary Information.[1] In the present case, the observed rate constant (k_2) approaches the association rate constant (k_a) because the electron transfer rate (k_{et}) is much larger than the dissociation rate constant (k_{-a}). Association is strongly ionic strength dependent,[49-53] because of the favorable electrostatic interactions between CcP and Cc. The results are shown in Figure 3.3 and Table S3.1. Interestingly, they show that Cc forms a productive, reactive complex at least as effectively with CcP_B as with CcP_A. At moderate ionic strength the rate constants are even slightly higher, indicating a more favorable interaction. Given the fact that the rates for the Cc-CcP_A interaction at low ionic strength are over 10^9 $M^{-1}s^{-1}$, and thus close to the diffusion limit, it is remarkable that with CcP_B Cc achieves even faster association. To check whether this could be explained by possible ET from Cc bound to the new encounter site in addition of ET in the stereospecific complex the edge-to-edge distance between Cc heme and the indole of the CcP compound I radical forming Trp (Trp-191) was measured for all Cc orientations observed in the Monte Carlo simulation of CcP_B (Figure 3.1d). All orientations of Cc in the new negative patch yield distances > 1.6 nm, suggesting that the rate of ET would be negligibly slow from this site. Shorter distances are only found for Cc binding near the stereospecific complex. Thus, to achieve ET Cc that binds at the new patch needs to diffuse to the binding site of the stereospecific complex to form a productive complex. It is concluded, therefore, that the additional charges enhance the chance of the formation of the productive complex, even though the new charges are on the side of CcP, relative to the stereospecific binding site (Figure 3.1). This is consistent with the idea that encounter complexes close to the binding site consist of productive encounters because they promote the formation of the stereospecific complex. [18]

Conclusions

In summary, an additional negative patch was introduced on the surface of CcP, lateral to its stereospecific binding site for Cc (Figure 3.1). Both the Monte Carlo calculations and the PRE data indicate that Cc interacts with the new patch, yet this does not perturb the formation of the stereospecific complex. Earlier work demonstrated that the natural electrostatic patch of CcP optimally directs Cc to the site of stereospecific complex.[22, 23, 26, 28, 37] However, an optimized distribution of the charges around the stereospecific binding site is apparently not critical. Cc molecules that bind at the new negative patch can find their way to the stereospecific binding site before dissociation of the encounter complex. The new site thus produces productive rather than futile encounters.[1, 41] CcP_B has a much larger negative charge compared to CcP_A. We conclude that the positive effect of the increased strength of the electrostatic interaction on the association rate outweighs the negative effect of a less optimized charge distribution.

References

(1) Schreiber, G., Haran, G., and Zhou, H. X. (2009) Fundamental aspects of protein-protein association kinetics, *Chem. Rev. 109*, 839-860.

(2) Ubbink, M. (2012) Dynamics in transient complexes of redox proteins, *Biochem. Soc. Trans. 40*, 415-418.

(3) Yang, J., Zeng, Y. F., Liu, Y. F., Gao, M., Liu, S., Su, Z. D., and Huang, Y. Q. Electrostatic interactions in molecular recognition of intrinsically disordered proteins, *J. Biomol. Struct. Dyn.*, 12.

(4) Zhou, H. X., and Pang, X. D. (2018) Electrostatic interactions in protein structure, folding, binding, and condensation, *Chem. Rev. 118*, 1691-1741.

(5) Clore, G. M. (2014) Interplay between conformational selection and induced fit in multidomain protein-ligand binding probed by paramagnetic relaxation enhancement, *Biophys. Chem. 186*, 3-12.

(6) Schilder, J., and Ubbink, M. (2013) Formation of transient protein complexes, *Curr. Opin. Struct. Biol. 23*, 911-918.

(7) Adam, G., and Delbrück, M. (1968) Reduction of dimensionality in biological diffusion processes, In *Structural Chemistry and Molecular Biology* (A. Rich, N. D., Ed.), p 198, W. H. Freeman and Co., San Francisco.

(8) Kim, Y. C., Tang, C., Clore, G. M., and Hummer, G. (2008) Replica exchange simulations of transient encounter complexes in protein-protein association, *Proc. Natl. Acad. Sci. U. S. A. 105*, 12855-12860.

(9) Van de Water, K., van Nuland, N. A. J., and Volkov, A. N. (2014) Transient protein encounters characterized by paramagnetic NMR, *Chem. Sci. 5*, 4227-4236.

(10) Scanu, S., Foerster, J. M., Ullmann, G. M., and Ubbink, M. (2013) Role of hydrophobic interactions in the encounter complex formation of the plastocyanin and cytochrome *f* complex revealed by paramagnetic NMR spectroscopy, *J. Am. Chem. Soc. 135*, 7681-7692.

(11) Sugase, K., Dyson, H. J., and Wright, P. E. (2007) Mechanism of coupled folding and binding of an intrinsically disordered protein, *Nature 447*, 1021-U1011.

(12) Camacho, C. J., Weng, Z., Vajda, S., and DeLisi, C. (1999) Free energy landscapes of encounter complexes in protein-protein association, *Biophys. J. 76*, 1166-1178.

(13) Camacho, C. J., Kimura, S. R., DeLisi, C., and Vajda, S. (2000) Kinetics of desolvation-mediated protein-protein binding, *Biophys. J. 78*, 1094-1105.

(14) Camacho, C. J., and Vajda, S. (2002) Protein-protein association kinetics and protein docking, *Curr. Opin. Struct. Biol. 12*, 36-40.

(15) Rajamani, D., Thiel, S., Vajda, S., and Camacho, C. J. (2004) Anchor residues in protein-protein interactions, *Proc. Natl. Acad. Sci. U. S. A. 101*, 11287-11292.

(16) Harel, M., Spaar, A., and Schreiber, G. (2009) Fruitful and Futile Encounters along the Association Reaction between Proteins, *Biophys. J. 96*, 4237-4248.

(17) Fawzi, N. L., Doucleff, M., Suh, J. Y., and Clore, G. M. (2010) Mechanistic details of a protein-protein association pathway revealed by paramagnetic relaxation enhancement titration measurements, *Proc. Natl. Acad. Sci. U. S. A. 107*, 1379-1384.

(18) Andralojc, W., Hiruma, Y., Liu, W. M., Ravera, E., Nojiri, M., Parigi, G., Luchinat, C., and Ubbink, M. (2017) Identification of productive and futile encounters in an electron transfer protein complex, *Proc. Natl. Acad. Sci. U. S. A. 114*, E1840-E1847.

(19) Strickland, M., Kale, S., Strub, M. P., Schwieters, C. D., Liu, J., Peterkofsky, A., and Tjandra, N. (2019) Potential regulatory role of competitive encounter eomplexes in paralogous phosphotransferase systems, *J. Mol. Biol. 431*, 2331-2342.

(20) Kale, S., Strickland, M., Peterkofsky, A., Liu, J., and Tjandra, N. (2019) Model of a kinetically driven crosstalk between paralogous protein encounter complexes, *Biophys. J. 117*, 1655-1665.

(21) An, S. Y., Kim, E.-H., and Suh, J.-Y. (2018) Facilitated protein association via engineered target search pathways visualized by paramagnetic NMR spectroscopy, *Structure 26*, 887-893.e882.

(22) Pelletier, H., and Kraut, J. (1992) Crystal structure of a complex between electron transfer partners, cytochrome *c* peroxidase and cytochrome *c*, *Science 258*, 1748-1755.

(23) Gabdoulline, R. R., and Wade, R. C. (2001) Protein-protein association: investigation of factors influencing association rates by Brownian dynamics simulations, *J. Mol. Biol. 306*, 1139-1155.

(24) Poulos, T. L., Freer, S. T., Alden, R. A., Edwards, S. L., Skogland, U., Takio, K., Eriksson, B., Xuong, N. H., Yonetani, T., and Kraut, J. (1980) Crystal-structure of cytochrome-*c* peroxidase, *J. Biol. Chem. 255*, 575-580.

(25) Louie, G. V., Hutcheon, W. L. B., and Brayer, G. D. (1988) Yeast iso-1-cytochrome *c*: A 2.8 Å resolution three-dimensional structure determination, *J. Mol. Biol. 199*, 295-314.

(26) Northrup, S., Boles, J., and Reynolds, J. (1988) Brownian dynamics of cytochrome *c* and cytochrome *c* peroxidase association, *Science 241*, 67-70.

(27) Volkov, A. N., Worrall, J. A. R., Holtzmann, E., and Ubbink, M. (2006) Solution structure and dynamics of the complex between cytochrome *c* and cytochrome *c* peroxidase determined by paramagnetic NMR, *Proc. Natl. Acad. Sci. U. S. A. 103*, 18945-18950.

(28) Bashir, Q., Volkov, A. N., Ullmann, G. M., and Ubbink, M. (2010) Visualization of the encounter ensemble of the transient electron transfer complex of cytochrome *c* and cytochrome *c* peroxidase, *J. Am. Chem. Soc. 132*, 241-247.

(29) Volkov, A. N., Bashir, Q., Worrall, J. A. R., Ullmann, G. M., and Ubbink, M. (2010) Shifting the equilibrium between the encounter state and the specific form of a protein complex by interfacial point mutations, *J. Am. Chem. Soc. 132*, 11487-11495.

(30) Geren, L., Hahm, S., Durham, B., and Millett, F. (1991) Photoinduced electron-transfer between cytochrome-*c* peroxidase and yeast cytochrome-*c* labeled at cys-102 with(4-bromomethyl-4'-methylbipyridine) bis(bypyridine) ruthenium^{2+}, *Biochemistry 30*, 9450-9457.

(31) Worrall, J. A. R., Kolczak, U., Canters, G. W., and Ubbink, M. (2001) Interaction of yeast iso-1-cytochrome *c* with cytochrome *c* peroxidase investigated by N-15,H-1 heteronuclear NMR spectroscopy, *Biochemistry 40*, 7069-7076.

(32) Miller, M. A., Liu, R. Q., Hahm, S., Geren, L., Hibdon, S., Kraut, J., Durham, B., and Millett, F. (1994) Interaction domain for the reaction of cytochrome-*c* with the radical and the oxyferryl heme in cytochrome-*c* peroxidase compound-I, *Biochemistry 33*, 8686-8693.

(33) Erman, J. E., Vitello, L. B., Pearl, N. M., Jacobson, T., Francis, M., Alberts, E., Kou, A., and Bujarska, K. (2015) Binding of yeast cytochrome *c* to forty-four charge-reversal mutants of yeast cytochrome *c* peroxidase: isothermal titration calorimetry, *Biochemistry 54*, 4845-4854.

(34) Pearl, N. M., Jacobson, T., Arisa, M., Vitello, L. B., and Erman, J. E. (2007) Effect of single-site charge-reversal mutations on the catalytic properties of yeast cytochrome *c* peroxidase: Mutations near the high-affinity cytochrome *c* binding site, *Biochemistry 46*, 8263-8272.

(35) Pearl, N. M., Jacobson, T., Meyen, C., Clementz, A. G., Ok, E. Y., Choi, E., Wilson, K., Vitello, L. B., and Erman, J. E. (2008) Effect of single-site charge-reversal mutations on the catalytic properties of yeast cytochrome *c* peroxidase: Evidence for a single, catalytically active, cytochrome *c* binding domain, *Biochemistry 47*, 2766-2775.

(36) Humphrey, W., Dalke, A., and Schulten, K. (1996) VMD: Visual molecular dynamics, *J. Mol. Graph. 14*, 33-38.

(37) Castro, G., Boswell, C. A., and Northrup, S. H. (1998) Dynamics of protein-protein docking: Cytochrome *c* and cytochrome *c* peroxidase revisited, *J. Biomol. Struct. Dyn. 16*, 413-424.

(38) Worrall, J. A. R., Liu, Y. J., Crowley, P. B., Nocek, J. M., Hoffman, B. M., and Ubbink, M. (2002) Myoglobin and cytochrome *b(5)*: A nuclear magnetic resonance study of a highly dynamic protein complex, *Biochemistry 41*, 11721-11730.

(39) Worrall, J. A. R., Reinle, W., Bernhardt, R., and Ubbink, M. (2003) Transient protein interactions studied by NMR spectroscopy: The case of cytochrome *c* and adrenodoxin, *Biochemistry 42*, 7068-7076.

(40) Xu, X. F., Reinle, W. G., Hannemann, F., Konarev, P. V., Svergun, D. I., Bernhardt, R., and Ubbink, M. (2008) Dynamics in a pure encounter complex of two proteins studied by solution scattering and paramagnetic NMR spectroscopy, *J. Am. Chem. Soc. 130*, 6395-6403.

(41) Clore, G. M., and Iwahara, J. (2009) Theory, practice, and applications of paramagnetic relaxation enhancement for the characterization of transient low-population states of biological macromolecules and their complexes, *Chem. Rev. 109*, 4108-4139.

(42) Otting, G. (2010) Protein NMR using paramagnetic ions, In *Annual Review of Biophysics* (Rees, D. C., Dill, K. A., and Williamson, J. R., Eds.), p 387, Annu. Rev. Biophys., Palo Alto.

(43) Volkov, A. N., Ubbink, M., and van Nuland, N. A. J. (2010) Mapping the encounter state of a transient protein complex by PRE NMR spectroscopy, *J. Biomol. NMR 48*, 225-236.

(44) Erman, J. E., Vitello, L. B., Mauro, J. M., and Kraut, J. (1989) Detection of an oxyferryl porphyrin π-cation-radical intermediate in the reaction between hydrogen peroxide and a mutant yeast cytochrome *c* peroxidase - Evidence for tryptophan-191 involvement in the radical site of compound I, *Biochemistry 28*, 7992-7995.

(45) Scholes, C. P., Liu, Y. J., Fishel, L. A., Farnum, M. F., Mauro, J. M., and Kraut, J. (1989) Recent ENDOR and pulsed electron paramagnetic resonance studies of cytochrome *c* peroxidase - Compound I and its site-directed mutants, *Isr. J. Chem. 29*, 85-92.

(46) Sivaraja, M., Goodin, D. B., Smith, M., and Hoffman, B. M. (1989) Identification by ENDOR of Trp191 as the free-radical site in cytochrome *c* peroxidase compound ES, *Science 245*, 738-740.

(47) Coulson, A. F. W., Erman, J. E., and Yonetani, T. (1971) Studies on cytochrome *c* peroxidase XVII. Stoichiometry and mechanism of the reaction of compound ES with donors, *J. Biol. Chem. 246*, 917.

(48) Summers, F. E., and Erman, J. E. (1988) Reduction of cytochrome *c* peroxidase compounds I and II by ferrocytochrome *c*. A stopped-flow kinetic investigation., *J. Biol. Chem. 263*, 14267-14275.

(49) Matthis, A. L., and Erman, J. E. (1995) Cytochrome *c* peroxidase-catalyzed oxidation of yeast iso-1 ferrocytochrome *c* by hydrogen peroxide. Ionic strength dependence of the steady-state parameters., *Biochemistry 34*, 9985-9990.

(50) Matthis, A. L., Vitello, L. B., and Erman, J. E. (1995) Oxidation of yeast iso-1 ferrocytochrome *c* by yeast cytochrome *c* peroxidase compounds I and II. Dependence upon ionic strength, *Biochemistry 34*, 9991-9999.

(51) Zhou, J. S., and Hoffman, B. M. (1994) Stern-Volmer in reverse: 2:1 stoichiometry of the cytochrome *c*-cytochrome *c* peroxidase electron-transfer complex, *Science 265*, 1693-1696.

(52) Van de Water, K., Sterckx, Y. G. J., and Volkov, A. N. (2015) The low-affinity complex of cytochrome *c* and its peroxidase, *Nat. Commun. 6*, 7073.

(53) McLendon, G., Zhang, Q., Wallin, S. A., Miller, R. M., Billstone, V., Spears, K. G., and Hoffman, B. M. (1993) Thermodynamic and kinetic aspects of binding and recognition in the cytochrome *c*/cytochrome *c* peroxidase complex, *J. Am. Chem. Soc. 115*, 3665-3669.

Chapter 3

Supplementary Information

Materials and Methods

Mutagenesis

The *Saccharomyces cerevisiae* CcP gene with mutation C128A to avoid dimerization and the sequence MKT at the N-terminus was considered as the wild-type gene (CcP_A)[1, 2] and sub-cloned in a pET28a(+) vector.[3] CcP_B additionally contained the mutations K21E, K29E, K90E, and K97E. The DNA construct was ordered from a commercial vendor. For PRE experiments, the mutations N24C, N87C and N200C were introduced one at a time in the CcP genes through site specific mutagenesis using the QuikChange method (Life technologies, Invitrogen, ThermoFisher). The sequence of constructs were verified by DNA sequencing.

Protein Production

CcP was produced in *E. coli* BL21 Star (DE3)pLysS (Life Technologies Europe BV, Bleiswijk, the Netherlands). The production and purification followed previously described protocols,[2-4] with some adaptations. The gradient for the elution during the anion-exchange chromatography for CcP_A was performed by mixing 50 mM potassium phosphate pH 5 and 500 mM potassium phosphate pH 5, while 500 mM KCl was added to the second buffer to elute CcP_B. *S. cerevisiae* Cc, either with or without ^{15}N labelling was produced using the iso-1-cytochrome *c* gene in a pUC19 based plasmid and purified as described.[3, 5, 6]

Tagging with MTS/MTSL

CcP was tagged with either MTS (1-acetoxy-2,2,5,5-tetramethyl-d3-pyrroline-3-methyl)-methanethiosulfonate) as diamagnetic tag (TRC, Canada) or MTSL (1-oxyl-2,2,5,5-tetramethyl-d3-pyrroline-3-methyl)-methanethiosulfonate) (ChemCruz, Santa Cruz Biotechnology, Texas) as paramagnetic tag, according to the published procedure.[1] It was found that the tagging efficiency was close to 100% according to mass spectrometry. However, after tagging not all labels remained paramagnetic according to electron paramagnetic resonance (EPR) spectroscopy, ranging between about 30% and 80% (Table S3.2). For the EPR measurement two samples were prepared in 20 mM sodium phosphate, 0.1 M NaCl, pH 6 buffer. One contained 140 µM MTSL tagged CcP and one 100 µM free MTSL, freshly dissolved for each experiment. The measurements were performed at 9.8 GHz, at room temperature, using 0.63 mW microwave power, 2 G modulation amplitude, 100 kHz modulation frequency and a time constant of 10.24 msec (Figure S3.4). The percentage of paramagnetic protein was calculated comparing the double integral of free MTSL and tagged CcP spectra. The error in the EPR measurement is estimated to be ± 5 percent points.

NMR Experiments

For titration experiments, NMR samples contained 200 μM of resting state CcP in 20 mM sodium phosphate, 0.1 M NaCl, pH 6 and 6% D_2O for lock. Oxidized ^{15}N Cc was titrated in ten aliquots into the CcP solution, increasing the ratio (Cc)/(CcP) progressively from 0.3 to 3. For PRE measurements, NMR samples contained ^{15}N Cc and MTS(L) labelled CcP in a 1:1 ratio and concentration of 200 μM in the same buffer. BEST-TROSY-HSQC[7] spectra were recorded on a Bruker AVIII HD 850 MHz spectrometer at 293 K with 0.333 sec relaxation delay, 64 scans and 1048 and 200 complex points in the ^1H and ^{15}N dimensions, respectively. It is noted that the paramagnetic relaxation also affects R_1 relaxation, which can lead to a larger recovery of magnetization for amide protons that experience paramagnetic relaxation. This effect can result in an underestimation of the PRE, and thus the PRE values should be considered lower limits. PREs are only interpreted qualitatively in this work and the effects are compared for CcP_A and CcP_B. Thus, a possible underestimation of the PRE does not affect the conclusions. Data processing was done in Topspin 4.0.6 (Bruker, Karlsruhe, Germany) and the data were analyzed with CCPN analysis version 2.4.0. Assignment of the ^{15}N, ^1H resonances of free Cc was based on literature data[8-10] (BMRB 17845). The chemical shift perturbations (CSP) were analyzed by overlaying the spectrum of free Cc with the spectra of Cc bound with CcP at different concentrations. The K_D was calculated by fitting the data to equation (1),[11] describing a 1:1 binding model:

$$\Delta\nu^{i} = \frac{1}{2}\Delta\nu^{0}\left(A - \sqrt{A^2 - \frac{4}{R}}\right) \qquad A = 1 + \frac{1}{R} + \frac{P_0 R + C_0}{R P_0 C_0 K_A} \qquad (1)$$

where P_0 is the starting concentration CcP, C_0 is the stock concentration of Cc, R is the ratio (Cc_i/CcP_i) at step i in the titration, $\Delta\nu^i$ is the chemical shift change at step i, $\Delta\nu^0$ is the maximal change in the chemical shift and K_A is the association constant ($1/K_D$). Fitting was done with OriginPro 9.1 (OriginLab, Northampton, USA). The average CSP were calculated as previously described.[12] The association constant was used to calculate the percentage of Cc bound to CcP in the samples with 1:1 ratio of CcP:Cc. Of Cc, 84% and 83% was bound to CcP_A and CcP_B, respectively. The average CSP for the 100% bound form of Cc was extrapolated dividing the average CSP observed by 0.84 or 0.83 respectively. The spectra were also analyzed with TITAN software,[13] after processing the time domain data with nmrpipe,[14] yielding lower limits for the dissociation rate constant, k_a, with K_D fixed at 6 μM.

For PRE analysis, the ratio between the intensity (peak heights) of the peaks of Cc in complex with CcP tagged with MTS or MTSL (I_{para}/I_{dia}) was used. All the I_{para}/I_{dia} were normalized using the intensity of the residues that were not affected by PRE (20% of the peaks). The uncertainties for the I_{para}/I_{dia} values of each amide were calculated by propagation of two times the standard deviation of the noise level of each spectrum. The PRE was calculated as previously described.[3, 15, 16] The PREs were corrected for the fraction

of Cc bound to CcP (83% to CcP_B and 84% to CcP_A) and for the percentage of paramagnetic signal of the tagged CcP as measured by EPR (see above and Table S3.2). The error in the R_2dia values were obtained by calculating two times the standard deviation of the R_2dia of several PRE experiments conducted on the complexes Cc:CcP_A or Cc:CcP_B respectively. A lower limit for the PRE was set to 5 s^{-1}, because smaller PREs cannot be measured accurately, while the upper limit was determined by the noise level of the spectrum, i.e. the lowest point from which the peaks in the paramagnetic spectrum are broadened beyond detection. These limits were scaled by dividing with the fraction of protein bound and the fraction of paramagnetic CcP as derived from the EPR signal.

Monte Carlo simulations of encounter complex ensemble

The structures of CcP and Cc were taken from the PDB 2PCC.[17] On both proteins hydrogen atoms were added with the module HBUILD[18] in the program CHARMM.[19] The positions of the heavy atoms were preserved while only the hydrogens were minimized with the CHARMM force field.[20] For the mutant CcP B four mutations, as stated in the experiment, were introduced: K21E, K29E, K90E, and K97E using Pymol.[21] The heme ligands of CcP and Cc were considered to be in the oxidized state. The electrostatic potential of CcP was calculated with the program APBS.[22] In order to include the solvent, the dielectric constants of the protein and the water were set to 4 and 80, respectively. The calculation was performed at 303 K and in the presence of 120 mM NaCl. The electrostatic potentials were saved on a grid with a diameter of 22.5 nm.

The electrostatic docking procedure was done with the program suite MCMap.[23] The protein CcP was considered as receptor while Cc as a ligand was moving randomly in the electrostatic field of CcP. The simulation consisted of 250 runs with 10^6 steps for each at a temperature of 303 K. For the resulting ensemble only encounters fulfilling the Metropolis MC criterion[24] were saved. To account for the encounter complex, different ensembles were created in which encounters within a distance of 0.3 nm to the surface of CcP or without a distance criterion were considered as valid encounter. For each resulting ensemble, randomly chosen 5000 encounters were used for further analysis. The resulting ensembles were analyzed more in detail for the possibility of an electron transfer reaction from CcP to Cc, from which the one with a surface distance of 0.3 nm was used further. An electron transfer reaction was considered as possible if the minimal edge-to-edge distance of the Trp191 indole of CcP to the heme of Cc was less than 1.6 nm.

Kinetic measurements

Immediately prior to the measurements, Cc was reduced with sodium ascorbate in 20 mM sodium phosphate solution, 270 mM NaCl, pH 8. Subsequently, using PD10 columns, both Cc and CcP were brought into a buffer containing 20 mM sodium phosphate solution and NaCl, pH 6 with the desired ionic strength, 752 mM, 622 mM, 502 mM, 392 mM, 292 mM, 192 mM or 122 mM NaCl. Resting state CcP was converted into compound I with 1 molar

equivalent H_2O_2 yielding a shift of the Soret band from 410 nm to 420 nm. Stopped-flow experiments were performed on a SX20 stopped flow spectrometer (AppliedPhotophysics, Leatherhead, Surrey, UK) with a 1.2 ms deadtime with a 1:1 concentration ratio of Cc and CcP, either 1 μM (concentration after mixing) for buffers with I = 752 mM to I= 292 mM or 0.5 μM for I = 192 mM and I = 122 mM . The kinetic traces were measured following the absorbance at 416 nm (oxidation of Cc, see Text S3.1). The change in absorbance (ΔA_{416}) was fitted to equation (2):

$$\Delta A_{416} = B_0 \cdot \Delta\varepsilon_{416} \cdot \left(1 - \frac{1}{1+k_2 \cdot B_0 \cdot t}\right) + C \qquad (2)$$

where B_0 is the starting concentration of Cc(II) and CpdI, $\Delta\varepsilon_{416}$ is the difference in extinction coefficient at 416 nm for oxidized and reduced Cc, -40 mM^{-1} cm^{-1} [25-27] and C corrects for the baseline voltage of the spectrometer. Equation 2 is based on the analytical solution of the differential equation for the change in concentrations of Cc(II) and CpdI in the case that the starting concentrations are equal and the stoichiometry of conversion is 1:1. It was used to obtain the bimolecular rate constant k_2, which depends on the rate constant of association (k_a), the dissociation rate constant (k_{-a}) and the electron transfer rate (k_{et}), equation (3):

$$k_2 = \frac{k_a k_{et}}{k_{-a}+k_{et}} \qquad (3)$$

Under the assumption that electron transfer is much faster than dissociation ($k_{-a} << k_{et}$), the observed rate approaches the association rate constant, $k_2 \approx k_a$.[28, 29] The analysis of the data was done with OriginPro 9.1 (OriginLab, Northampton, USA). Every curve resulted from the average of fourteen single measurements. The reported k_a is the average of at least three curves each fitted to the equation 2. The curves presented an artifact at the beginning of the measurement, probably due to the mixing phase, which was not considered in the fitting (Figure S3.3). Since the equation used to fit the kinetics assumes a 1:1 ratio in concentration between Cc and CcP and due to the complexity of the Cc:CcP cycle, just the rapid decay caused by the oxidation of Cc(Fe^{+2}) was fitted to obtain the k_a. In the second part the curves, other reactions can have a relevant influence on the absorbance at 416 nm, particularly the conversion of CpdII to CcP. The errors in the rate constants represent the standard deviation between the rates obtained from the single fits at each salt concentration (Table S3.1).

Supporting Text

Text S3.1. Affinity and binding of Cc is similar for CcP_A and CcP_B

NMR spectroscopy was used to compare the general characteristics of binding of Cc to CcP_B with binding to CcP_A experimentally. ^{15}N labelled Cc was titrated into a solution of unlabeled CcP and the effects on the ^{15}N-^{1}H HSQC spectrum were analyzed. At a low

ratio of Cc to CcP, most Cc is in the bound state and with increasing ratio more Cc is in the free state. The resonances shifted during the titration, indicating that Cc binding and release are in the fast-exchange regime.[30] The sizes and direction of the chemical shift perturbations (CSP) were similar in both titrations (Figure S3.2), indicating that the mode of binding is similar. The dissociation constant was K_D of 6 (±1) × 10^{-6} M in both cases (Figure S3.1), in line with other reports.[3, 30-32] Line shape analysis using TITAN software[13] with the K_D fixed to 6 μM yields a lower limit of the dissociation rate constant of ~6,400 s^{-1}.

Text S3.2. Reaction cycle and stopped flow measurements

The reaction catalyzed by CcP consists of the reduction of H_2O_2 to water using electrons transferred from Cc. The reaction proceeds through a complicated cycle, during which two molecules of Cc interact with CcP, each sequentially contributing one electron.

$$CcP(Fe^{3+}) + H_2O_2 \rightarrow CpdI + H_2O \qquad (r1)$$

$$CpdI + Cc(Fe^{2+}) \xrightarrow{k(I)} CpdII + Cc(Fe^{3+}) \qquad (r2)$$

$$CpdII + Cc(Fe^{2+}) \xrightarrow{k(II)} CcP(Fe^{3+}) + Cc(Fe^{3+}) \qquad (r3)$$

During this process, CcP reduces hydrogen peroxide forming the intermediate called compound I (CpdI), which, after receiving one electron from Cc, is converted into compound II (CpdII). Finally, a second molecule of reduced Cc donates one electron to CpdII restoring the resting state of CcP.[33]

The kinetics were measured by following the absorbance at 416 nm for both the Cc:CcP_A and Cc:CcP_B complexes. The kinetics at 416 nm reflect all reactions involving the oxidation of $Cc(Fe^{+2})$ by CpdI or CpdII (Figure S3.3). The reduction of CpdI to CpdII constitutes the reduction of the Trp radical which does not result in spectral changes in the visible region. Note that the kinetics are measured at a ratio of 1:1 between Cc(II) and CpdI. This allows other reactions between the different species in solution to happen as soon as part of the CpdI molecules have been reduced by Cc, such as reaction (r3) or the dismutation reaction between two CpdII molecules:

$$CpdII + CpdII \xrightarrow{k(III)} CpdI + CcP$$

For this reason, only the first part of the stopped-flow traces was fitted (Figure S3.3).

Supporting Figures

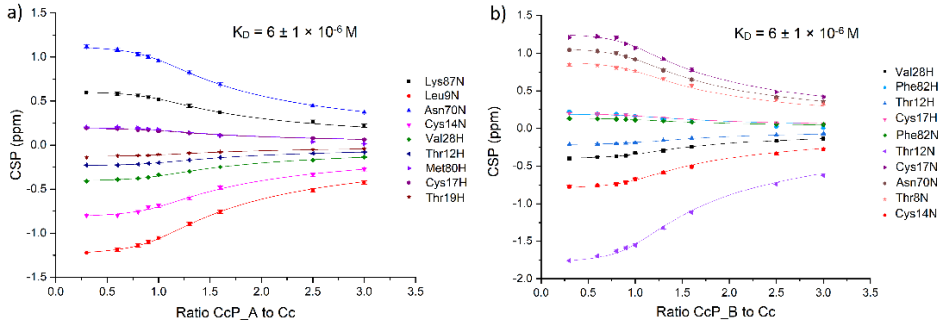

Figure S3.1. Affinity between Cc and CcP. Titration curves for ^{15}N ferric Cc and CcP_A (a) or CcP_B (b). The CSP for several ^{1}H and ^{15}N nuclei of Cc are plotted as a function of the ratio CcP and Cc. The lines represent global fits with a shared K_D, indicated above the plots.

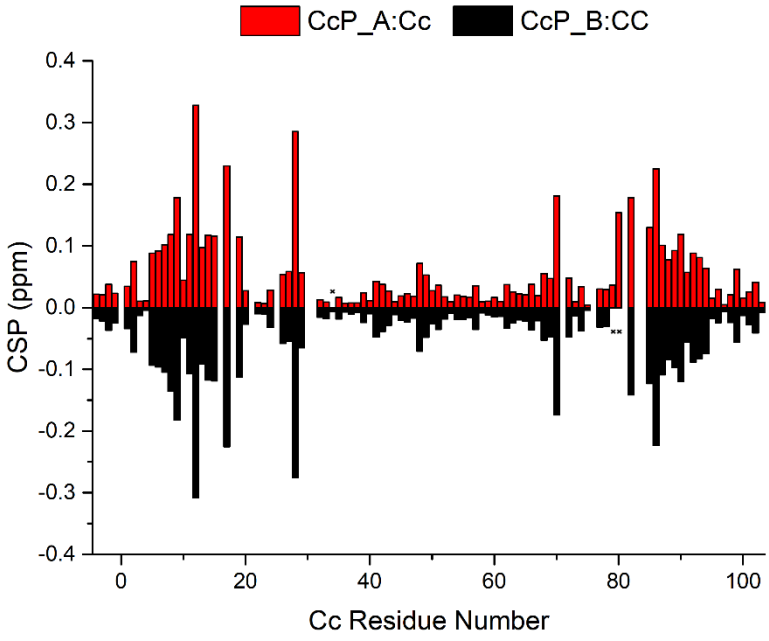

Figure S3.2. Chemical shift perturbations upon complex formation. Comparison of the average CSP extrapolated to the 100% bound state for the complexes CcP_A:Cc (red) and CcP_B:Cc (black). The small black crosses indicate residues for which no data are available.

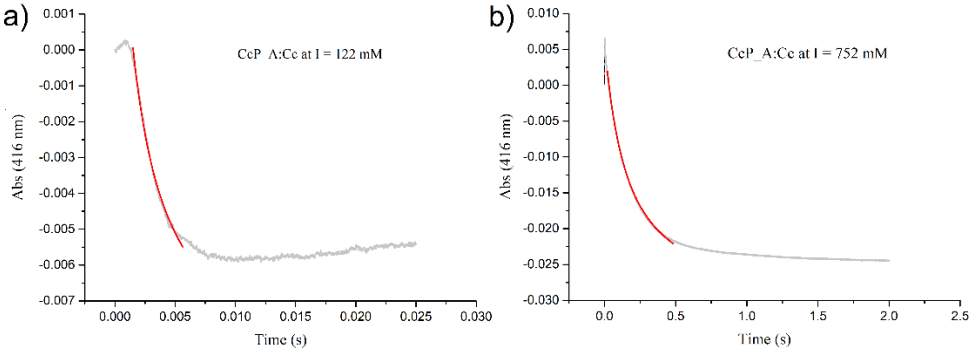

Figure S3.3. Representative stopped flow data. Kinetic traces for the reaction between Cc and CcP_A at low (a) and high (b) ionic strength. Experimental data is in grey, fit to equation 2 is in red.

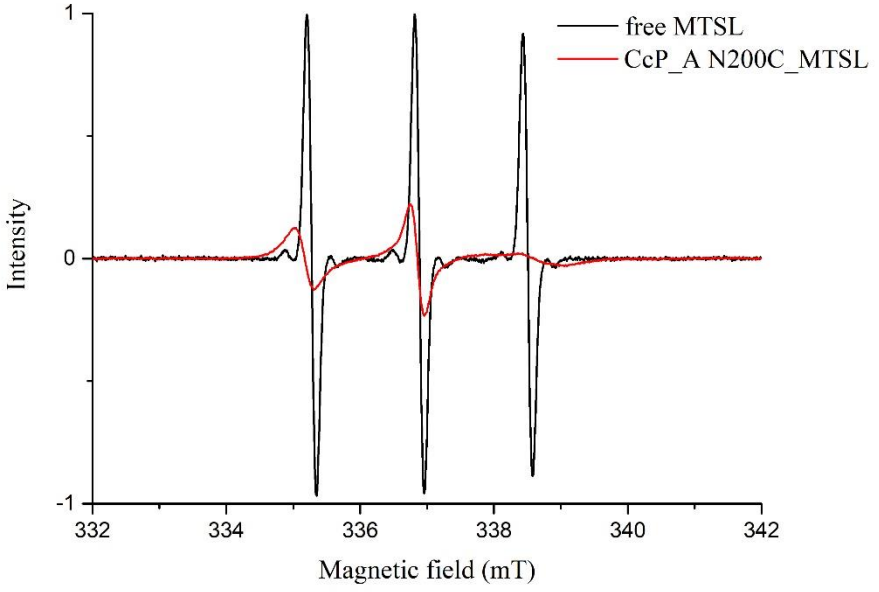

Figure S3.4. EPR spectra used to establish the fraction of paramagnetic CcP after labelling with MTSL. The spectra were normalized for concentration and number of scans. The measurements were performed at 9.8 GHz at room temperature, using 0.63 mW microwave power, 2 G modulation amplitude, 100 kHz modulation frequency and a time constant of 10.24 msec.

Supporting Tables

Table S3.1. Rate constants for the reaction of the Cc:CcP_A and Cc:CcP_B complexes. The error represents the standard error of the mean between the curves at each salt concentration.

	CcP_A		CcP_B	
Ionic strength (mM)	**k_a ($M^{-1}s^{-1}$)**	**standard error (%)**	**k_a ($M^{-1}s^{-1}$)**	**standard error (%)**
752	$6.2*10^6$	9.4	$7.1*10^6$	5.0
622	$1.2*10^7$	4.4	$1.3*10^7$	5.2
502	$2.4*10^7$	4.4	$3.3*10^7$	8.6
392	$4.5*10^7$	3.4	$5.8*10^7$	3.9
292	$1.5*10^8$	1.8	$2.1*10^8$	5.9
192	$6.8*10^8$	7.3	$8.5*10^8$	3.9
122	$1.5*10^9$	4.7	$2.1*10^9$	17.3

Table S3.2. Percentage of paramagnetic signal of CcP tagged with MTSL measured through EPR experiments. The error is estimated to be ± 5 percent points.

	N24C	**N87C**	**N200C**
CcP_A	59%	28%	82%
CcP_B	45%	35%	50%

References

(1) Volkov, A. N., Worrall, J. A. R., Holtzmann, E., and Ubbink, M. (2006) Solution structure and dynamics of the complex between cytochrome *c* and cytochrome *c* peroxidase determined by paramagnetic NMR, *Proc. Natl. Acad. Sci. U. S. A. 103*, 18945-18950.

(2) Goodin, D. B., Davidson, M. G., Roe, J. A., Mauk, A. G., and Smith, M. (1991) Amino-acid substitutions at tryptophan-51 of cytochrome-*c* peroxidase - Effects on coordination, species preference for cytochrome *c*, and electron-transfer, *Biochemistry 30*, 4953-4962.

(3) Schilder, J., Lohr, F., Schwalbe, H., and Ubbink, M. (2014) The cytochrome *c* peroxidase and cytochrome *c* encounter complex: The other side of the story, *FEBS Lett. 588*, 1873-1878.

(4) Teske, J. G., Savenkova, M. I., Mauro, J. M., Erman, J. E., and Satterlee, J. D. (2000) Yeast cytochrome *c* peroxidase expression in *Escherichia coli* and rapid isolation of various highly pure holoenzymes, *Protein Expr. Purif. 19*, 139-147.

(5) Pollock, W. B., Rosell, F. I., Twitchett, M. B., Dumont, M. E., and Mauk, A. G. (1998) Bacterial expression of a mitochondrial cytochrome *c*. Trimethylation of lys72 in yeast iso-1-cytochrome *c* and the alkaline conformational transition, *Biochemistry 37*, 6124-6131.

(6) Morar, A. S., Kakouras, D., Young, G. B., Boyd, J., and Pielak, G. J. (1999) Expression of N-15-labeled eukaryotic cytochrome *c* in *Escherichia coli*, *J. Biol. Inorg. Chem. 4*, 220-222.

(7) Lescop, E., Schanda, P., and Brutscher, B. (2007) A set of BEST triple-resonance experiments for time-optimized protein resonance assignment, *J. Magn. Reson. 187*, 163-169.

(8) Gao, Y., Boyd, J., Williams, R. J. P., and Pielak, G. J. (1990) Assignment of proton resonances, identification of secondary structural elements, and analysis of backbone chemical shifts for the C102T variant of yeast iso-1-cytochrome *c* and horse cytochrome *c*, *Biochemistry 29*, 6994-7003.

(9) Fetrow, J. S., and Baxter, S. M. (1999) Assignment of 15N chemical shifts and 15N relaxation measurements for oxidized and reduced iso-1-cytochrome *c*, *Biochemistry 38*, 4480-4492.

(10) Volkov, A. N., Vanwetswinkel, S., Van de Water, K., and van Nuland, N. A. J. (2012) Redox-dependent conformational changes in eukaryotic cytochromes revealed by paramagnetic NMR spectroscopy, *J. Biomol. NMR 52*, 245-256.

(11) Kannt, A., Young, S., and Bendall, D. S. (1996) The role of acidic residues of plastocyanin in its interaction with cytochrome *f*, *BBA - Bioenergetics 1277*, 115-126.

(12) Grzesiek, S., Bax, A., Clore, G. M., Gronenborn, A. M., Hu, J. S., Kaufman, J., Palmer, I., Stahl, S. J., and Wingfield, P. T. (1996) The solution structure of HIV-1 Nef reveals an unexpected fold and permits delineation of the binding surface for the SH3 domain of Hck tyrosine protein kinase, *Nat. Struct. Biol. 3*, 340-345.

(13) Waudby, C. A., Ramos, A., Cabrita, L. D., and Christodoulou, J. (2016) Two-dimensional NMR lineshape analysis, *Sci. Rep-UK 6*, 8.

(14) Delaglio, F., Grzesiek, S., Vuister, G. W., Zhu, G., Pfeifer, J., and Bax, A. (1995) NMRPIPE - A multidimensional spectral processing system based on Unix Pipes, *J. Biomol. NMR 6*, 277-293.

(15) Bashir, Q., Volkov, A. N., Ullmann, G. M., and Ubbink, M. (2010) Visualization of the encounter ensemble of the transient electron transfer complex of cytochrome *c* and cytochrome *c* peroxidase, *J. Am. Chem. Soc. 132*, 241-247.

(16) Battiste, J. L., and Wagner, G. (2000) Utilization of site-directed spin labeling and high-resolution heteronuclear nuclear magnetic resonance for global fold determination of large proteins with limited nuclear Overhauser effect data, *Biochemistry 39*, 5355-5365.

(17) Pelletier, H., and Kraut, J. (1992) Crystal structure of a complex between electron transfer partners, cytochrome *c* peroxidase and cytochrome *c*, *Science 258*, 1748-1755.

(18) Brunger, A. T., and Karplus, M. (1988) Polar hydrogen positions in proteins: empirical energy placement and neutron diffraction comparison., *Proteins 4*, 148-156.

(19) Brooks, B. R., Bruccoleri, R. E., Olafson, B. D., States, D. J., Swaminathan, S., and Karplus, M. (1983) CHARMM: A program for macromolecular energy, minimization, and dynamics calculations., *J. Comput. Chem. 4*, 187-217.

(20) MacKerell, A. D., Bashford, D., Bellott, M., Dunbrack, R. L., Evanseck, J. D., Field, M. J., Fischer, S., Gao, J., Guo, H., Ha, S., Joseph-McCarthy, D., Kuchnir, L., Kuczera, K., Lau, F. T. K., Mattos, C., Michnick, S., Ngo, T., Nguyen, D. T., Prodhom, B., Reiher, W. E., Roux, B., Schlenkrich, M., Smith, J. C., Stote, R., Straub, J., Watanabe, M., Wiorkiewicz-Kuczera, J., Yin, D., and Karplus, M.

(1998) All-atom empirical potential for molecular modeling and dynamics studies of proteins, *J. Phys. Chem. B 102*, 3586-3616.

(21) Schrödinger, L. The PyMOL Molecular Graphics System, Version 1.3.

(22) Jurrus, E., Engel, D., Star, K., Monson, K., Brandi, J., Felberg, L. E., Brookes, D. H., Wilson, L., Chen, J. H., Liles, K., Chun, M. J., Li, P., Gohara, D. W., Dolinsky, T., Konecny, R., Koes, D. R., Nielsen, J. E., Head-Gordon, T., Geng, W. H., Krasny, R., Wei, G. W., Holst, M. J., McCammon, J. A., and Baker, N. A. (2018) Improvements to the APBS biomolecular solvation software suite, *Protein Sci. 27*, 112-128.

(23) Foerster, J. M., Poehner, I., and Ullmann, G. M. (2018) MCMap-Computational tool for mapping energy landscapes of transient protein-protein interactions, *ACS Omega 3*, 6465-6475.

(24) Metropolis, N., Rosenbluth, A. W., Rosenbluth, M. N., Teller, A. H., and Teller, E. (1953) Equation of state calculations by fast computing machines., *J. Chem. Phys. 21*, 1087-1092.

(25) Hahm, S., Miller, M. A., Geren, L., Kraut, J., Durham, B., and Millett, F. (1994) Reaction of horse cytochrome-*c* with the radical and the oxyferryl heme in cytochrome-*c* peroxidase compound-I, *Biochemistry 33*, 1473-1480.

(26) Coulson, A. F., Erman, J. E., and Yonetani, T. (1971) Studies on cytochrome *c* peroxidase. XVII. Stoichiometry and mechanism of the reaction of compound ES with donors, *J. Biol. Chem. 246*, 917-924.

(27) Ho, P. S., Hoffman, B. M., Kang, C. H., and Margoliash, E. (1983) Control of the transfer of oxidizing equivalents between heme iron and free radical site in yeast cytochrome *c* peroxidase, *J. Biol. Chem. 258*, 4356-4363.

(28) Ho, P. S., Hoffman, B. M., Solomon, N., Kang, C. H., and Margoliash, E. (1984) Kinetics and energetics of intramolecular electron-transfer in yeast cytochrome-*c* peroxidase, *Biochemistry 23*, 4122-4128.

(29) Schreiber, G., Haran, G., and Zhou, H. X. (2009) Fundamental aspects of protein-protein association kinetics, *Chem. Rev. 109*, 839-860.

(30) Worrall, J. A. R., Kolczak, U., Canters, G. W., and Ubbink, M. (2001) Interaction of yeast iso-1-cytochrome *c* with cytochrome *c* peroxidase investigated by N-15,H-1 heteronuclear NMR spectroscopy, *Biochemistry 40*, 7069-7076.

(31) Matthis, A. L., and Erman, J. E. (1995) Cytochrome *c* peroxidase-catalyzed oxidation of yeast iso-1 ferrocytochrome *c* by hydrogen peroxide. Ionic strength dependence of the steady-state parameters., *Biochemistry 34*, 9985-9990.

(32) Corin, A. F., Hake, R. A., McLendon, G., Hazzard, J. T., and Tollin, G. (1993) Effects of surface amino acid replacements in cytochrome *c* peroxidase on intracomplex electron transfer from cytochrome *c*, *Biochemistry 32*, 2756-2762.

(33) Kim, K. L., Kang, D. S., Vitello, L. B., and Erman, J. E. (1990) Cytochrome-*c* peroxidase catalyzed oxidation of ferrocytochrome-*c* by hydrogen-peroxide - Ionic-strenght dependence of the steady-state rate parameters, *Biochemistry 29*, 9150-9159.